All-optical multifunctional logic operations using simultaneously both interferometric output ports in a symmetric SOA-MZI

Cláudia Reis[1*], Tanay Chattopadhyay[2], Giorgia Parca[1], Rogério Dionísio[3,1], Paulo André[1,4] and António Teixeira[1,5]

[1]Instituto de Telecomunicações, Campus de Santiago, 3810-197, Aveiro, Portugal
[2]Kolaghat Thermal Power Station, WBPDCL, 721137, West Bengal, India
[3]Escola Superior de Tecnologia de Castelo Branco (ESTCB), Avenida do empresário, 6000-767 Castelo Branco, Portugal
[4]Departamento de Física, Universidade de Aveiro, Campus Universitário de Santiago, 3810-193 Aveiro, Portugal
[5]Departamento de Electrónica, Telecomunicações e Informática, Universidade de Aveiro, Campus Universitário de Santiago, 3810-193 Aveiro, Portugal
[*]Corresponding author's E-mail: creis@av.it.pt

Abstract:

In this paper, all-optical logic functions, implemented with a single SOA-based Mach-Zehnder interferometer (SOA-MZI), are demonstrated experimentally and through numerical simulations. The proposed optical configuration is capable to carry out four logic operations, using simultaneously both output ports of the SOA-MZI. This may reduce the power cost and make possible to obtain simultaneously multi logic functions. The performance of such architecture is assessed measuring the obtained extinction ratio (ER) for each Boolean function.

The potential of integration makes the proposed scheme attractive to perform optical signal processing operations in next generation photonic transmission systems.

Subject Terms: All-optical signal processing, Mach-Zehnder interferometer, all-optical logic gates, semiconductor optical amplifier.

1. Introduction

In the last few years, the exponential growth of network traffic motivated the development of ultrafast signal processing in the optical domain [1]. In this context, all-optical logic gates are essential devices since they can execute complex optical processing functions, from binary address and header recognition to optical time division demultiplexing, which demonstrates their importance in a wide range of applicability.

Recently, all-optical logic gates have been widely investigated and several approaches have been experimentally demonstrated namely using a nonlinear optical loop mirror (NOLM) [2], a highly Ge-doped nonlinear fiber with a TeraHertz optical asymmetric demultiplexer [3] or using two microring resonators [4]. In [5] and [6-8] Sagnac interferometric structures and SOA-based Mach-Zehnder interferometers are also used, respectively, to perform several all-optical logic operations. The SOA-MZI is a highly versatile element that can perform a variety of optical logic functions and can provide high ER, requires low switching energies to operate, has regenerative capability and low-switching window (3.5-8 ps).

Logical operation using a single SOA-MZI switch is an attractive technology due to the small device size and low power consumption. Also it is less complex than other all-optical logic gate designs. Depending on the signals applied into its input ports, a single SOA-MZI switch is capable to carry out different logic operations at the same time, using simultaneously both output ports of the SOA-MZI. Traditional logic gates have a single output, but if we take advantage of the two output ports of the SOA-MZI based interferometric switch as logical

outputs, it is possible to obtain multi output logic functions. Using this concept, some theoretical designs have been proposed recently [9-12].

In this paper, four all-optical logic operations (And, Transposed Inhibition, Equivalence, Inverter) based on a single hybrid integrated SOA-MZI are simulated and experimentally demonstrated, using NRZ-OOK modulated signals driven at 10 Gbit/s.

This paper is organized as follows: in Section 2, we demonstrate four Boolean optical operations based on a single SOA-MZI. Their operation principle is explained through the analysis of the truth table and a black box model for operational point optimization. The experimental results obtained are presented on Section 3. Finally, in Section 4, the conclusions are drawn.

2. All-optical logic operations based on a symmetrical SOA-MZI switch

2.1 Operation principle

Four Boolean operations (And, Transposed Inhibition, Equivalence, Inverter) can be performed depending of the signals applied into the input ports #a, #b and #c of the interferometric structure illustrated in Fig.1. At the output ports #I and #J, optical band pass filters are placed in order to recover the signal injected into port #b.

Table 1 represents the truth table of the proposed circuit and from this table it is possible to obtain the logical expression at the output ports. Therefore, the Boolean equations at the interferometric output ports, expressed in the disjunctive canonical form, are given by

$$\begin{aligned} I &= a \cdot b \cdot \bar{c} + \bar{a} \cdot b \cdot c \\ J &= \bar{a} \cdot b \cdot \bar{\bar{c}} + a \cdot b \cdot c \end{aligned} \tag{1}$$

Where the symbols '$\cdot$' and '$\bar{}$' indicate logical 'And' and 'Inverter/Not'expression, respectively. Equations (1) are already in their simplified form, so it is not necessary to use Karnaugh maps or apply Boolean algebra to obtain a simpler solution.

Consider two modulated signals X=[10010000] and Y=[00010010], at the same wavelength, and a continuous signal at a different wavelength. If signals X and Y are injected, respectively, at port #a and port #b of the SOA-MZI switch (no signal at port #c), according to equation (1) the logical expressions at the output ports can be written as

$$\begin{aligned} I &= X \cdot Y \cdot \bar{0} + \overline{X} \cdot Y \cdot 0 = X \cdot Y \\ J &= \overline{X} \cdot Y \cdot \overline{0} + X \cdot Y \cdot 0 = \overline{X} \cdot Y \end{aligned} \tag{2}$$

which correspond to the logic 'And' and 'Transposed inhibition' operations between the two modulated optical beams. Also, based on this case, an 'Equivalence' and 'Not' logic operations can be obtained, simultaneously, at port #I and port #J of the SOA-MZI if the signal X is launched at port #a and the continuous signal at port #b. In this situation, the logic equations at the interferometric output ports are

$$\begin{aligned} I &= X \cdot 1 \cdot \bar{0} + \overline{X} \cdot 1 \cdot 0 = X \\ J &= \overline{X} \cdot 1 \cdot \overline{0} + X \cdot 1 \cdot 0 = \overline{X} \end{aligned} \tag{3}$$

On the other hand, if signal Y is injected at port #c while at port #b we maintain the continuous wave signal, the logical expressions at the output ports #I and #J can be written according to equation (1) as

$$\begin{aligned} I &= 0 \cdot 1 \cdot \overline{Y} + \bar{0} \cdot 1 \cdot Y = Y \\ J &= \bar{0} \cdot 1 \cdot \overline{Y} + 0 \cdot 1 \cdot Y = \overline{Y} \end{aligned} \tag{4}$$

From these two latter cases, we can conclude that if a control signal is injected at port #a or port #c of the SOA-MZI, the two even parts of the continuous wave signal (injected at port

#b) will propagate through the two MZI arms and will suffer different gains and phase shifts, leading to the unbalance of the SOA-MZI. In these cases, the modulation of the refractive index will not be the same ($n_{SOA1} \neq n_{SOA2}$) and the light in the upper arm of the MZI will present a different velocity than the lower arm; hence a replica of the control signal appear at port #I (Equivalence operation), and its complementary at port #J (Not operation). In this paper, the Not operation is designed using a very simple logic circuit since it is performed using only two optical signals (one modulated and another continuous), contrary to the Not implementations that uses three optical signals.

2.2 Black box static model

The all-optical logic operations proposed in this paper are based on the symmetrical SOA-MZI switch shown in Fig. 1, where each arm incorporates one Semiconductor Optical Amplifier (SOA_1 or SOA_2) and one Phase Shifter (PS_1 or PS_2).

The proposed configuration operates on the principle of optically induced phase shift on a carrier signal and is controlled essentially by the power level propagating along the arms, the SOA's operational parameters and by the PSs. The power distribution along the device affects the output interference depth and its potential optimization, which is a crucial parameter since it determines the switching efficiency of the SOA-MZI.

The device was characterized experimentally in terms of non-ideal splitting factors and SOA1, 2 gains, following the method adopted in [13].

The measurements of SOA-MZI output power as function of input power and SOA current were made considering the two arms separately, using forward propagation, from input #a to output #I, with SOA2 disabled and, similarly, from input #c to output #J, with SOA1 disabled.

The trends of the SOA output power vs. SOA current and input power were found and the obtained curves are shown in Fig. 2 a) and Fig. 2 b). It is worth noting that this characterization is referred to the overall path on which the signal propagates, so it takes into account losses and any other kind of asymmetry of the device.

The power at the output of the SOA-MZI (#I and #J) is a result of an interference process occurring in coupler α. The electromagnetic fields at the two inputs of this coupler will define the conditions for the outputs measured. So, specifically, when used as an amplitude modulator, one important factor to take into consideration is the ER of the output signal. For example, through SOAs input power/current variation, the power distribution on the SOA-MZI arms can be further changed, leading to the consequent variation of the interference conditions on output couplers.

Moreover, a phase shift on SOAs output signals is induced due to the dependence of SOAs refractive index on carrier density.

We model the working characteristic for a SOA-MZI, in order to describe how physical parameters actually control the interference depth, thus providing a tool for operational point optimization, which for example can be used for maximizing ER.

The output powers P_I (port #I) and P_J (port #J) are indirectly computed as a function of the SOAs' total input power level and SOAs' bias current (Isoa) through SOA 1,2 gain curves reported in Fig.2.

In Table 2, all the 3-bit words obtained combining the 0-1 levels on the inputs #a, #b, #c are considered and identified through the index i=1,…8.

A black box model, representing the relation between #I and #J output power as function of input power on port #b, obtained from interferometric structure principles considering the couplers yield, path differences and non-ideality, is given by:

$$\begin{aligned} P_{I_i} &= (1-\alpha)P_{1b_i} + \alpha P_{2b_i} - \sqrt{P_{1b_i} P_{2b_i}} \sin(\Delta\phi_i + s_{1_i}) \\ P_{J_i} &= \alpha P_{1b_i} + (1-\alpha)P_{2b_i} + \sqrt{P_{1b_i} P_{2b_i}} \sin(\Delta\phi_i + s_{2_i}) \\ \Delta\phi_i &= \Delta\phi_{a_i} - \Delta\phi_{c_i} + \Delta\phi_{b_0} = kP_a - kP_c + \frac{\pi}{2} \end{aligned} \quad (5)$$

Where α is the splitting factor of the last coupler, evaluated experimentally [13]. P_{1bi} and P_{2bi} are the power levels on λ_b at the input of the rightmost coupler in Fig. 1. $\Delta\phi_i$ is the phase difference between the two arms, which depends on the individual phase shift induced by the input #a on upper arm $\Delta\phi_{a_i}$, input #c on lower arm $\Delta\phi_{c_i}$ and input #b $\Delta\phi_{b_0}$ on both arms. The first two are considered linear with the respective input power, because of the linear relation between SOA induced phase and carrier density, through refractive index variation, taking into account that the SOAs' current was kept constant. The last phase shift is considered constant at the value $\frac{\pi}{2}$ due to the initial balancing operation which will be explained in the following. The other internal couplers yield, path length differences between the upper and lower arms, the SOA carrier density variations and non-ideality of the tested architecture, are taken into account through further phase delays s_{1i} and s_{2i}.

The SOA-MZI black box static model provides a general frame of how parameters control the interference depth, thus providing a tool for operational point optimization, which for example can be used for maximize the ER.

The parameters' values of the black box model, α estimated experimentally and the others through MATLAB, are reported in Table 3 and used for the final validation, carried out considering the measured output powers P_I and P_J, with $Isoa_1$ and $Isoa_2$ constant at 240 mA.

When the SOA-MZI depicted in Fig.1 is tested, the first operation performed is the balancing of the device, which consists in the maximization of the output ER (i.e. output port #J is maximized in power, whereas the output port #I is minimized, null in principle), by injecting a CW optical signal in the common input (port #b) at λ_b and adjusting the SOA-MZI operational parameters. After balancing the SOA-MZI, the basic switching operation is performed injecting a signal on port #a or #c: this will produce the interference inversion so that the injected signal will be forwarded through port #I, while the power on port #J is minimized.

In order to verify the logical operations, we use MATLAB environment and the black box model. At the output ports we measured the power levels corresponding to the expected logic operation on the wavelength of the signal injected in #b input, λ_b. Thus, in all the cases where port #b is set to zero, no wavelength conversion was performed.

In Fig.3, we present the comparison among the obtained experimental static power measurements shown in Table 1 and the modeled output power levels. Through the static black box model, it was possible to find a good matching with the correct output levels, applying the optimization of all the parameters that affect the output interference, exactly as it happens experimentally when the maximum ER between the port #I and #J has to be achieved.

The ER optimization is strictly dependent on each inputs combination, due to the different XGM/XPM effect induced by the two SOAs. The 4^{th} case (input combination=111),

illustrated in Fig. 3, explains how the power levels and the ER are reduced in practice because of the gains saturation and the presence of the three inputs a#, b#, c# set at logical level 1.

The interference depth can be maximized in theory and in practice through adjustments of the phase shifters contribution; in our formulation for the static model we included their contributions in the parameters $s_{1_i}$and s_{2_i}.

For all these reasons, the ER maximization in practice is obviously achieved differently for each case. This is why, for example, cases 2 (input combination=011) and 3 (input combination=110) are slightly different in power levels and ER, although the input configuration is the same, except for injecting signal at input #c in case 2 and at input #a in case 3.

3. Experimental results

To experimentally demonstrate different logic functions using both interferometric output ports of the SOA-MZI, we implemented the setups depicted in Fig. 4. They consist of two DFB lasers peaking at 1549.32 nm and 1547.72 nm, followed by polarizations controllers to adjust the input polarization. The laser at 1549.32 nm is optically modulated by a Mach–Zehnder operating at 10 Gbit/s, with an ER of 11dB, amplified by an Erbium Doped Fiber Amplifier (IPG-EAD-500-C3-W) and then split into two equal parts using a 3 dB coupler. The control data sequence is equal to X=[10010000] and is produced by a BERT pattern generator (Agilent N4901B). Different data patterns, launched into the SOA-MZI ports (CIP 100G-2R2-ORP), are obtained by delaying the X signal, using an optical delay line.

The signal at 1547.72 nm works in continuous wave (CW), and its power is adjusted by a variable optical attenuator (VOA).

The output signals are obtained using a filter with a 40 GHz bandwidth (X-tract Net Test), centered at the wavelength of the signal injected in port #b of the SOA-MZI.

A PIN (HP-11982A), with responsivity of 0.7 A/W, and an oscilloscope (Agilent Infinium 86100A) are used to analyze the temporal evolution of the different all-optical logic operations.

Initially, the SOA-MZI was balanced by acting on the SOAs gain and on the voltage of the phase shifters, so that in the absence of modulated control signals, the continuous wave signal injected in port #b could experience a complete destructive interference at port #I.

From the experimental setup depicted in Fig. 4a) we obtain the results of the all-optical And gate operation shown in Fig. 5. In this case, the modulated signals X and Y are respectively launched into port #a and port #b and, at the interferometric output ports, we obtain simultaneously the logical functions $I = X \cdot Y$ and $J = \overline{X} \cdot Y$. The measured ER for these two all-optical logic functions was 12.4 dB at port #I and 12.2 dB, at port #J.

In Fig. 4b) and Fig. 4c), the CW signal is injected at port #b of the SOA-MZI, and the control modulated signals X and Y are, respectively, injected at port #a in Fig. 4b) and at port #c in Fig. 4c) in order to obtain the Not operation and its complementary. Fig. 6 shows the results of the all-optical Not logical gate operation and its complementary: the left figure shows the results when the control signal X is injected in port #a of the SOA-MZI and the right figure when the control signal Y is injected at port #c. The ER for each of these logic functions was also experimentally analyzed and when the control signal X is injected we obtained 10.5 dB at port #I and 14 dB at port #J; when the control signal Y is injected we obtained 10 dB at port #I and 11.8 dB at port #J.

The experimental results show, in general, extinction ratio values higher than 10 dB, which proves the potential of using both output ports of the SOA-MZI to obtain, simultaneously And/Transposed Inhibition and Equivalence/Inverter logic functions.

4. Conclusions

This work experimentally demonstrates four all-optical logic operations, using simultaneously both output ports of a SOA-MZI. The experimental and simulation results confirm that the proposed configuration switch operates according to its truth table. The extinction ratio measurements also demonstrated the suitability of the proposed circuit for all-optical logic gates implementation.

Acknowledgement: This paper was supported by the FP7 Network of Excellence project EURO-FOS and the authors acknowledge the project CITO PTDC/EEA-TEL/114838/2009.

References

1. K.E. Zoiros, T. Houbavlis, M. Kalyvas, “Ultra-high speed all-optical shift registers and their applications in OTDM networks”, Opt Quant Electron 36(11), pp. 1005–1053, (2004).
2. Y. Miyoshi, K. Ikeda, H. Tobioka, I. Takashi, S. Namiki, K. Kitayama, “Ultrafast all-optical logic gate using a nonlinear optical loop mirror based multi-periodic transfer function”, Opt. Express 16(4), pp. 2570-2577, (2008).

3. M. P. Fok, P. R. Prucnal, “All-optical XOR gate with optical feedback using highly Ge-doped nonlinear fiber and a terahertz optical asymmetric demultiplexer,” Appl. Opt. 50(2), pp. 237–241 (2011).
4. L. Zhang, R. Ji, Y. Tian, L. Yang, P. Zhou, Y. Lu, W. Zhu, Y. Liu, L. Jia, Q. Fang, M. Yu, “Simultaneous implementation of XOR and XNOR operations using a directed logic circuit based on two microring resonators”, Opt. Express 19(7), pp. 6524-6540, (2011).
5. Y. Zhou, J. Wu, J. Lin, “Novel ultrafast all-optical XOR scheme based on Sagnac interferometric structure“, IEEE Journal of Quantum Electronics, 41(6), pp. 823-827, (2005).
6. J. M. Martinez, F. Ramos “10 Gb/s reconfigurable optical logic gate using a single hybrid-integrated SOA-MZI”, Fiber and Integrated Optics, 27(1), pp. 15-23, (2008).
7. J.-Y. Kim, J.-M. Kang, T.-Y. Kim, S.-K. Han, “All-optical multiple logic gates with XOR, NOR, OR, and NAND functions using parallel SOA-MZI structures: theory and experiment”, Journal of Lightwave Technology, 24(9), pp. 3392-3399, (2006).
8. X. Ye, P. Ye, M. Zhang, “All-optical NAND gate using integrated SOA-based Mach–Zehnder interferometer”, Optical Fiber Technology, 12 (4), pp. 312-316, (2006).
9. T.Chattopadhyay, “All-optical modified Fredkin gate”, IEEE Journal of Selected Topics in Quantum Electronics, 18(2), (2012), 585-592.
10. E. Dimitriadou and K.E. Zoiros, “On the design of ultrafast all-optical NOT gate using quantum-dot semiconductor optical amplifier-based Mach–Zehnder interferometer”, Optics and laser technology, 44(3), (2012), 600-607.

11. E. Dimitriadou and K.E. Zoiros, “On the feasibility of ultrafast all-optical NAND gate using single quantum-dot semiconductor optical amplifier-based Mach–Zehnder interferometer”, Optics and laser technology, 44(6), (2012), 1971-1981.
12. E. Dimitriadou and K.E. Zoiros, “Proposal for all-optical NOR gate using single quantum-dot semiconductor optical amplifier-based Mach–Zehnder interferometer”, Optics communications, 285(7), (2012), 1710-1716.
13. G. Parca, R. Dionísio, C. Reis, S. Betti, G. TosiBeleffi, A. Teixeira, “Inherent Fabrication Yields and Asymmetries Impacts on MZI-SOA Static Modeling”, ICTON 2010.

Table Caption:

Table 1: Truth table of the proposed all-optical circuit. #a, #b, #c: interferometric input ports; #I, #J: interferometric output ports.

Table 2: Possible input combinations.

Table 3: Parameters extracted from the model fittings and used in the final validation.

Figure caption:

Fig 1: Schematic diagram of the proposed all-optical circuit based on a single SOA-MZI. BPF: Band pass filter, PS: Phase shifter, SOA: Semiconductor optical amplifier. The input ports of the SOA-MZI are #a, #b, #c and the output ports are #I, #J.

Fig. 2: #I and #J output power as function of (a) SOA_1, SOA_2 current variation and (b) #a, #c input power.

Fig. 3: Comparison between measured and modeled output power levels versus #a, #b, #c input logic levels (level 0→0 mW; level 1→ 0.5 mW).

Fig. 4: Experimental setups: a) to obtain $I = X \cdot Y$ and $J = \overline{X} \cdot Y$; b) to obtain $I = X$ and $J = \overline{X}$; c) to obtain $I = Y$ and $J = \overline{Y}$.

Fig. 5: Experimental time domain traces obtained for Boolean functions $I = X \cdot Y$ and $J = \overline{X} \cdot Y$.

Fig. 6: Experimental time domain traces obtained for Boolean functions: on the left $I = X$ and $J = \overline{X}$; on the right $I = Y$ and $J = \overline{Y}$.

TABLES

Table 1

Expected logic levels					Experimental static power measurements (dBm)	
Inputs			Outputs			
a	**b**	**c**	**I**	**J**	**I**	**J**
0	0	0	0	0	-12,2	-12,2
0	0	1	0	0	-12,1	-13,7
0	1	0	0	1	-10,4	9,1
0	1	1	1	0	7,5	-8,7
1	0	0	0	0	-13,7	-12,2
1	0	1	0	0	-13,7	-12,4
1	1	0	1	0	7,9	-8,2
1	1	1	0	1	-11,2	2,4

Table 2

Input	***i =1***	***i =2***	***i =3***	***i =4***	***i =5***	***i =6***	***i =7***	***i =8***
#a	*0*	*0*	*1*	*1*	*0*	*0*	*1*	*1*
#b	*1*	*1*	*1*	*1*	*0*	*0*	*0*	*0*
#c	*0*	*1*	*0*	*1*	*0*	*1*	*0*	*1*

Table 3

α	k	$\Delta\phi_{b_0}$	s_{1_i}	s_{2_i}
0.51	*6.3e3*	$\frac{\pi}{2}\ rad$	$-1 \div 2\ rad$	$-1 \div 2\ rad$

Fig.1

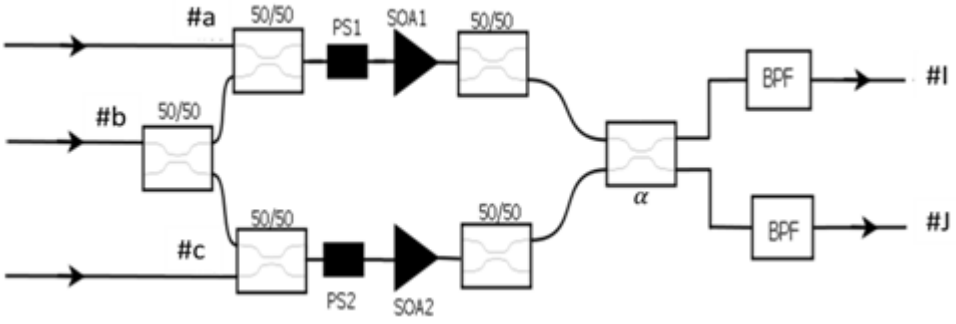

Fig. 2

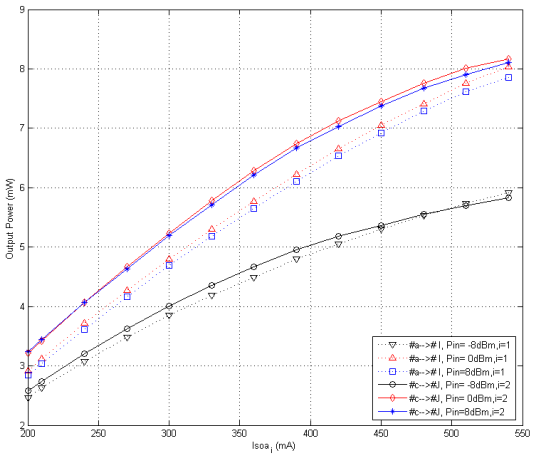
Output Power (mW)
Isoa_1 (mA)
#a->#1, Pin= -8dBm,i=1
#a->#1, Pin= 0dBm,i=1
#a->#1, Pin=8dBm,i=1
#c->#J, Pin= -8dBm,i=2
#c->#J, Pin= 0dBm,i=2
#c->#J, Pin=8dBm,i=2

(a)

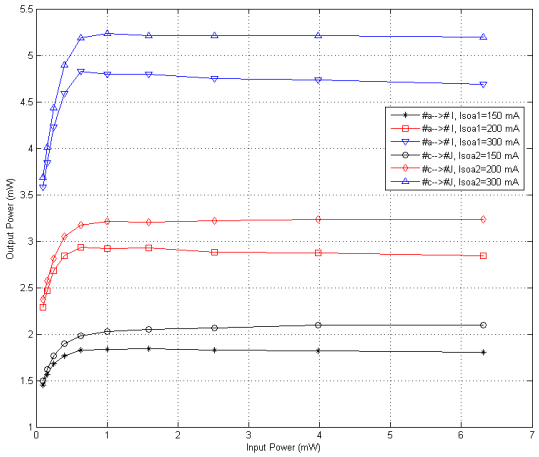
Output Power (mW)
Input Power (mW)
#a->#1, Isoa1=150 mA
#a->#1, Isoa1=200 mA
#a->#1, Isoa1=300 mA
#c->#J, Isoa2=150 mA
#c->#J, Isoa2=200 mA
#c->#J, Isoa2=300 mA

(b)

Fig. 3

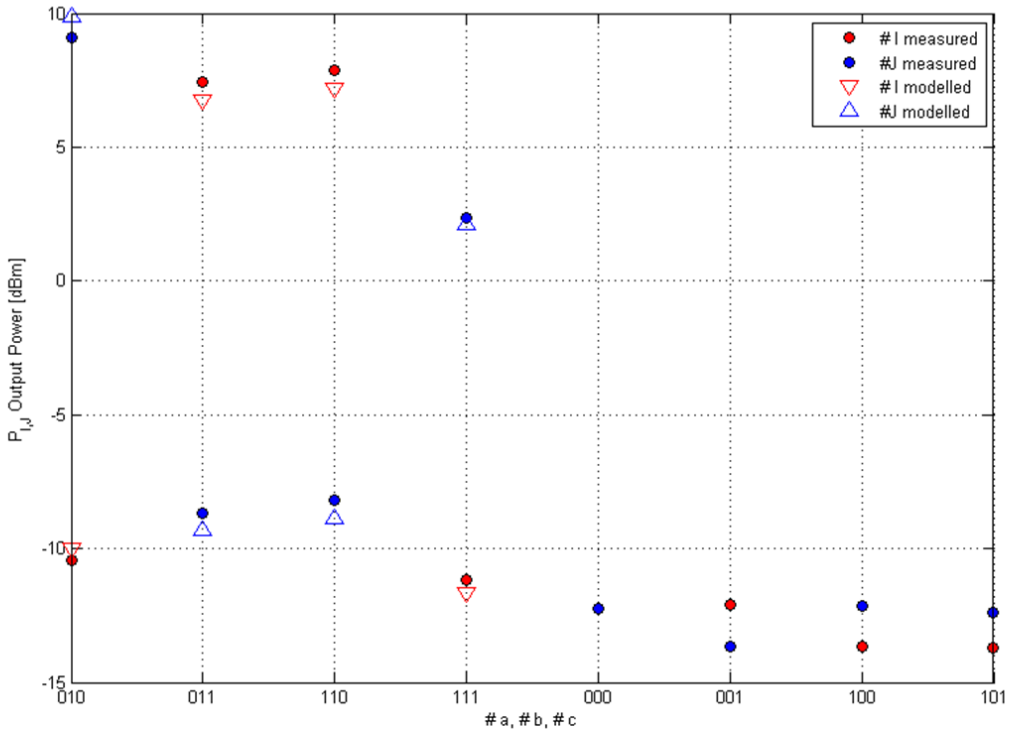

#a	#b	#c	#I	#J
X	Y	-	$X \cdot Y$	$\bar{X} \cdot Y$
X	CW	-	X	$\bar{X}$
-	CW	Y	Y	$\bar{Y}$

$$\#I = a \cdot \mathrm{b} \cdot \bar{c} + \bar{a} \cdot \mathrm{b} \cdot c$$

$$\#J = \bar{a} \cdot \mathrm{b} \cdot \bar{c} + a \cdot \mathrm{b} \cdot c$$

Fig. 4

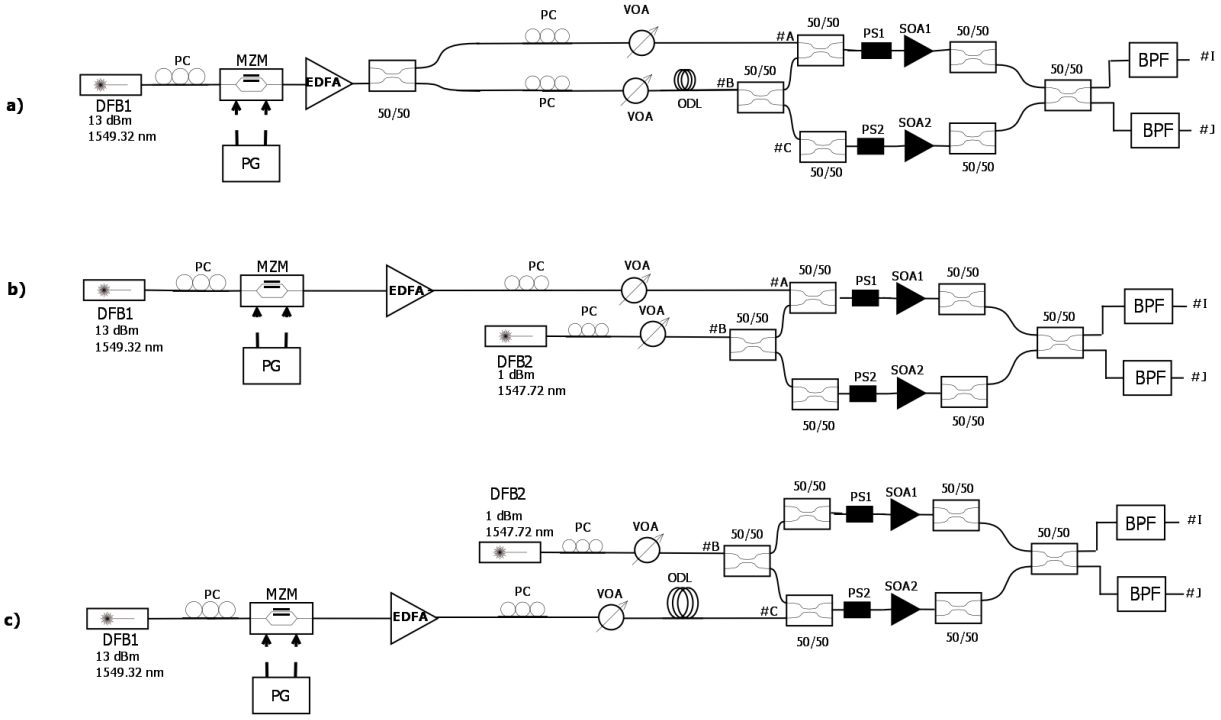
a)
DFB1
13 dBm
1549.32 nm
PC
MZM
PG
EDFA
50/50
PC
VOA
PC
VOA
ODL
#A
#B
#C
50/50
PS1
SOA1
PS2
SOA2
BPF
#I
#J
b)
DFB2
1 dBm
1547.72 nm
c)

Fig. 5

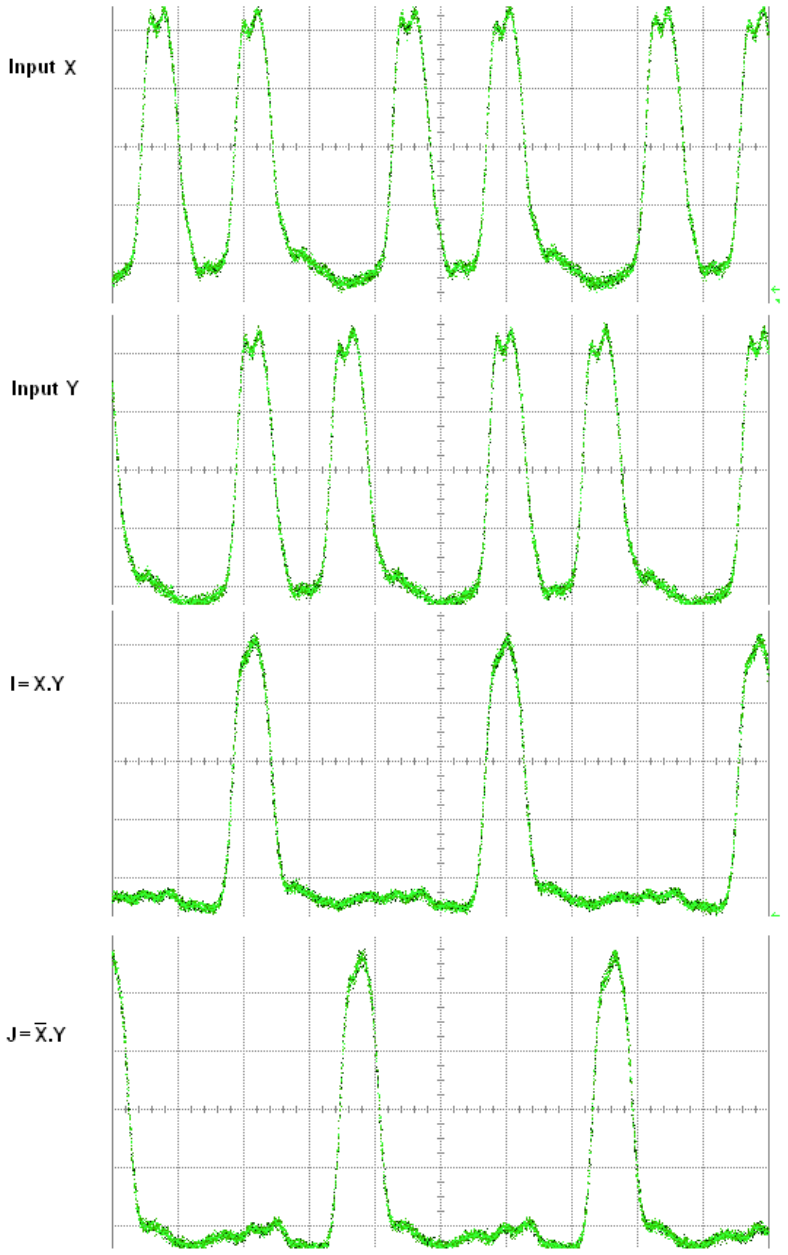

Fig. 6